Infrared Dichroism, Chain Flattening, and the Bound Fraction Histogram in Adsorbed Poly(methyl methacrylate) Layers

Peter Frantz and Steve Granick*

Department of Materials Science and Engineering, University of Illinois, Urbana, Illinois 61801

Received March 7, 1995; Revised Manuscript Received July 12, 1995[⊗]

ABSTRACT: We examine the distribution of adsorption substates, in contrast to their average. The distribution of infrared dichroism and bound fraction were determined in a model system (poly(methyl methacrylate) adsorbed chiefly by hydrogen bonding onto oxidized silicon from CCl_4). The method was infrared spectroscopy in attenuated total reflection (FTIR-ATR). From the surface excess (Γ), dichroic ratio (D_{zx}), and fraction of carbonyl groups bound to the surface (p), a broad distribution of conformations was found to prevail, from severely flattened ($p \approx 0.5$ and $D_{zx} \ll 1$ for the asymmetric methyl stretch) to nearly solution-like ($p \approx 0.1$ and $D_{zx} \approx 1$ for the asymmetric methyl stretch). The extent of flattening depended mainly on the number of adsorption sites available to each chain at the time it deposited to the surface; chains that adsorbed later, finding fewer and fewer surface sites available, then became attached by fewer and fewer segments. This in turn implied that chains which arrived initially had the center-of-mass closer to the solid surface than those which arrived later. Conformational rearrangements were not observed on the experimental time scale of 3 h; this allowed determination of the distribution of conformational substates by subtraction of sequentially-acquired infrared spectra. The broad and asymmetric distribution of conformational substates appeared to originate, predictably, from the piecemeal process by which the surface was coated. It presents analogies with issues of random sequential adsorption.

Introduction

The last two decades have seen rapid progress in understanding macromolecular interfacial properties. Advances in theory, experiment, and simulation have constructed an exhaustive description of the equilibrium composition and structure of an adsorbed layer based upon the relative free energies of adsorption.[1-4] However, a common admonition, which has echoed throughout these works, reminds us that deviations from this equilibrium picture will arise when the adsorbed layer loses its mobility.[1,2,4] Steric constraints and tenacious segment–surface interactions may hinder relaxation from nonequilibrium conformations. The potentially profound influence of a "glassy" sublayer on the composition, structure, and dynamics has been stressed.[5] The term "glassy" has come to be synonymous with a persistent nonequilibrium state. Indeed, it is evident in principle that a path to the state of lowest energy might not be available.

We distinguish three time scales in the development of an adsorbed layer: For diffusion to an initially bare surface, for attachment to the surface, and for equilibration of the adsorbed chains. The rate of each individual process is intimately coupled to that of the others. The composition and structure of the layer depend sensitively on the relative kinetics of these processes, as well as the traditional thermodynamic quantities (for example: the segment–surface interaction enthalpy, χ_s, the solution concentration, ϕ_s, and the degree of polymerization, n).[1] While the influence of the thermodynamic quantities is well understood, less is definitively known about kinetic properties. The primary motivation for this study is to investigate the behavior of a model system which, due to its limited surface mobility,[6-9] is expected to be restricted from structural equilibration *via* the third of the time scales alluded to above. Ultimately, we hope to contribute to the understanding of how kinetic and conformational properties are related.

Previous work on these questions took the approach of probing structure through its kinetic response. In pioneering experiments by Pefferkorn, Varoqui, and coworkers,[10,11] experiments were conceived to study the adsorption of tritium-labeled polystyrene ($M_w = 3.6 \times 10^5$) onto silica beads from dilute carbon tetrachloride. They first mapped out a peculiar adsorption isotherm with two distinct regions. It was postulated that the first region, a plateau for solution concentrations less than roughly 10 μg-mL^{-1}, indicated that the polystyrene was tightly bound in an almost flat conformation. The second region, in which the adsorbed mass grew with increasing concentration, indicated growth in the number of segments contained in loops and tails. Thus, it was possible to produce adsorbed layers with a variable fraction of segments bound to the surface.

The second experiment sought to determine the intrinsic self-mobility of the polymers composing these structurally distinct layers by finding, in each case, the mean time that a chain occupied the surface. This was done by measuring the rates of mass flux into the solution during displacement by an isotopically distinguishable molecule. This exchange was much slower for the tightly bound layer, occurring with a characteristic time of $\approx$20 h. They concluded that because of the restricted mobility, the layer was essentially frozen in a metastable state.

Additional evidence of long-lived nonequilibrium conformational states has been accumulating in our laboratory.[6-9,12-16] We have investigated the interfacial properties of a variety of model polymer/solvent systems adsorbed to a single solid oxidized surface. Surface excess (Γ), kinetics of adsorption and desorption, bound fraction (p), and the segment–surface interaction enthalpy (χ_s) have been some of the parameters directly accessible to us. From these measured kinetic and thermodynamic quantities, we have inferred changes in the composition and structure of adsorbed layers and

[⊗] Abstract published in *Advance ACS Abstracts,* September 1, 1995.

0024-9297/95/2228-6915$09.00/0

the dynamics which precipitate this evolution from one state to another.

But all of the above studies were based on indirect inferences as to surface structure; kinetics, not structure, was actually measured. In this paper we present direct evidence of persistent nonequilibrated structures within an adsorbed layer. Measurements of the mean segmental orientation, D_{zx}, combined with knowledge of the bound fraction, show that the first chains on the surface lay in a predominantly flattened conformation while the later chains arrived progressively more isotropic. This entropically unfavorable situation was observed to persist throughout the duration of our experiment (3 h), resisting the conformational equilibration found in less tenaciously bound polymers.[12,13] Finally, from spectral subtraction, estimates were made of the shape of the conformational distribution.

Experimental Section

Sample Cell for ATR. The surface excess, bound fraction, and dichroic ratio of poly(methyl methacrylate) (PMMA) adsorbed to oxidized silicon were monitored *in situ* during adsorption from dilute solution in carbon tetrachloride (CCl_4). Infrared spectra were collected using a Bio-Rad FTS-60 Fourier transform infrared spectrometer (FTIR) equipped with a broad-band mercury–cadmium–telluride (MCT) detector. Experiments were performed in the mode of attenuated total reflection (ATR). Related work was described by Flournoy and Shaffers,[17] and a similar apparatus was applied to the study of adsorbed polymer by Van Alsten[18] and by Sung.[19] The ATR element was mounted inside a stainless steel jacket thermostated at 30 °C.

The ATR cell, designed to provide laminar flow up to very high shear rates, was placed in a compartment external to the FTIR spectrometer. Reasons to work outside the standard sample compartment were essentially 3-fold. Most importantly, the volume of the standard compartment was too small for needed accessories. Second, the capability was desired to change the angle of incidence into the ATR crystal, requiring mobility of the detector and associated optics. Optics that would fit neatly into the spectrometer chamber are too "fast" (low f ratio) for sensitive angular-dependent work; to customize the optics, it was necessary to work outside. Finally, to attain precise temperature control over a wide temperature range would have been a formidable task in the same metal case that contains the infrared source and sensitive electronics.

Accordingly, experiments were performed in a nitrogen-purged external compartment which had been fitted with slow optics in order to obtain enhanced angular resolution of the sampling beam. Before impinging on the ATR crystal surface, the beam passed through a gold wire grid polarizer (Graesby/Specac). This consisted of a polished BaF_2 window with parallel gold wires spaced every 0.25 μm. Here BaF_2 was chosen because of all the available polarizer materials, it transmits the widest range of infrared radiation.

The ATR optical element was a rectangular trapezoid of dimensions 50 mm × 20 mm × 2 mm. The beam entrance surfaces were cut to either a 45 or 30° angle. The beam was reflected roughly 7 times as it traveled the length of the crystal. At the exit, the beam may be considered to be diverging from a point located on the exit face of the crystal. It then propagated toward an off-axis (90°) ellipsoidal mirror. This mirror focused the beam to a point on the MCT crystal of the detector.

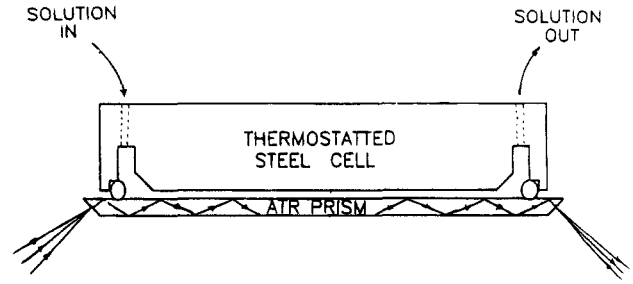

Figure 1. Schematic illustration of the infrared flow cell apparatus. The infrared beam sustains multiple internal reflections as it travels the length of a silicon prism. At each internal reflection, an evanescent wave penetrates to a depth of a few microns and suffers losses due to the excitation of vibrational modes of the material in the surface region. The flow cell is designed to produce laminar flow. The polymer solution is exposed to the top surface of the ATR prism.

Table 1. Characterization of the Poly(methyl methacrylates) (Suppliers' data)

sample	M_w	M_w/M_n	source
protio	107 000	1.10	Polymer Laboratories
	1 300 000	1.06	Polymer Laboratories
deuterio	90 000		Polymer Standards Services, Mainz, Germany

Figure 1 shows a schematic diagram of the stainless steel, thermostated flow cell. A special point of design was a specially-manufactured O-ring, composed of Viton (alternatively, polyisoprene) encased by Teflon. A tight seal was necessary to prevent leakage of liquid. This was usually provided by an aluminum plate clamped on the back, separated from the ATR plate by a silvered Viton gasket. Silver, which reflected the IR evanescent wave, was needed to avoid otherwise-huge IR absorbances in the 1700 cm^{-1} region.

Cell Preparation. The protocol for cleaning the cell and crystal may be found in ref 13, and preparation of the oxidized silicon surface in refs 13 and 20. The latter treatment has been shown[20] to reproducibly cultivate an oxidized surface (primarily SiO_2 and SiOH), while minimizing the amount of organic contamination from the ambient laboratory.

Polymer Samples. Anionically polymerized PMMA, protio and deuterio standards of various degrees of polymerization, were purchased from polymer laboratories and were used as received. Characteristics of these flexible linear chains are listed in Table 1. The net segment–surface interaction energy, evaluated by us using the method of Cohen Stuart et al.,[21] is 4 kT at 25 °C (k is the Boltzmann constant and T is the absolute temperature). This system shows no adsorption isotope effect.[6]

In these experiments with dilute carbon tetrachloride solution (spectroscopic grade CCl_4 was purchased from Sigma–Aldrich and used as received), the penetration depth of the infrared evanescent wave in the s-polarization was $d(p)_s = 0.76$ μm, and in the p-polarization $d(p)_p = 1.52$ μm, at the carbon–oxygen stretching frequency of 1732 cm^{-1}. At every wavelength, the evanescent wave sampled the interfacial region to a depth far larger than the thickness of the adsorbed layer (ca. the radius of gyration). Therefore the measured polymer peak intensities did not contain information about segment distribution as a function of depth but represented the surface excess of adsorbed polymer *in toto*.

Calibration of the Mass Adsorbed. Calibrations of the mass adsorbed per area (surface excess), and

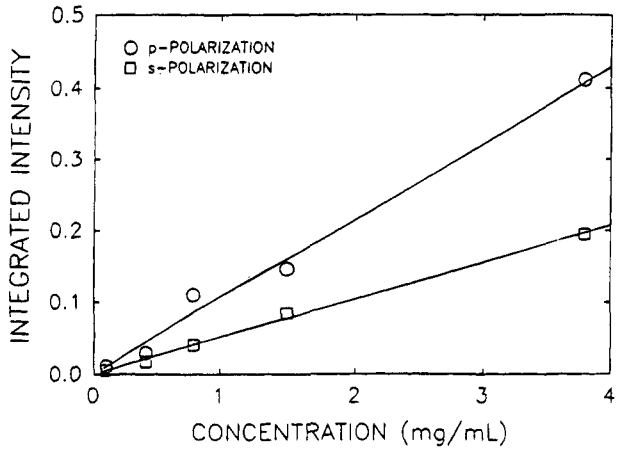

Figure 2. Calibration of mass adsorbed. Integrated intensity is plotted against concentration of the PMMA solution. The crystal used in this experiment was coated with a methyl-terminated monolayer (OTE) to prevent adsorption to the substrate. In an actual experiment, the integrated intensity at the experimental solution concentration is subtracted from the measurement in order to determine the infrared intensity attributable to the surface excess of polymer. The inverse of the slope of this calibration line is proportional to the constant of proportionality between surface excess (mass per area) and infrared absorption intensity exclusive of solution contributions.

corrections for the contribution from oscillators in solution, are described elsewhere for the simpler geometry of a cylindrical ATR crystal,[6] in which the polarization of the IR beam is not preserved. For a flat plate crystal it was necessary to calibrate the p- and s-polarizations independently.

The absorbance of a band in ATR geometry has been described by Harrick[22,23] and Tompkins;[24] calibration has been described by Arribart.[25] Here the concentration profile of oscillators normal to the surface, $c(z)$, is approximated by a delta function for the surface layer (thickness $\ll d_p$, the penetration depth of the evanescent wave) and a second term to represent the contribution of oscillators in solution. Straightforward arguments then show that the infrared absorption intensity is similarly composed of the sum of two terms: a term representing the surface excess and a second term, proportional to solution concentration, representing the contribution of oscillators in solution.

The constant of proportionality is determined by performing a simple experiment. First, the surface coverage, Γ, is held to zero by preventing adsorption (e.g., by covering the surface with a methyl-terminated monolayer, such as OTE[26]). The absorbance is then measured as a function of solution concentration, c_s, as in Figure 2, with a separate calibration for each polarization direction.

Conversion into mass adsorbed then basically follows the methods described in refs 6 and 25. The main difference, with polarized as against unpolarized radiation, is that a differing abundance of oscillators contributes to the ATR signal. Because s-polarization samples two directions of space, the isotropic solution contributes an oscillator density proportional to $(2/3)c_s$. Similarly, because p-polarization samples a single direction of space, the isotropic solution contributes an oscillator density proportional to $(1/3)c_s$. The geometrical definitions of s- and p-polarizations are shown in Figure 3.

The absorptivity of hydrogen-bonded carbonyl groups exceeds that of free carbonyl groups, as discussed in ref 6.

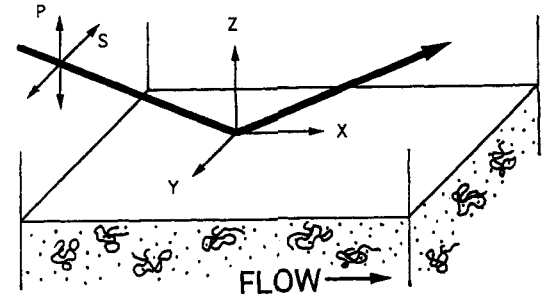

Figure 3. Illustration of the coordinate system. The ATR intensities (A_s and A_p) for plane-polarized radiation are related to the three components of the absorption index, A_x, A_y, and A_z. Here, x indicates the direction of flow as solution is injected into the cell, y is also in the plane of the surface, but perpendicular to the flow, and z is the direction normal to the surface.

Calibration of the Dichroic Ratio. Long ago, concurrent with the development of the ATR technique, Flournoy and Schaffers described the polarized spectroscopy of anisotropic films.[17] The analysis is based just on Maxwell's equations, Fresnel's equation, Snell's law, and the assumptions first that the real part of the refractive index is isotropic and, secondly, that the imaginary part is small (but anisotropic). The ATR intensities (A_s and A_p) of plane-polarized radiation are then related to the three components of the adsorption index, A_x, A_y, A_z:

$$A_s = \alpha A_y \tag{1}$$

$$A_p = \beta A_x + \gamma A_z \tag{2}$$

Here the coefficients α, β, and γ are known functions of the refractive indices and the angle of incidence. The orientations of these indices with respect to the crystal surface are shown in Figure 3. Here x and y are in the plane of the surface and z is normal to the surface.

Considerable effort is required to extricate the three spatial adsorption indices from the two Flournoy–Schaffers equations. A technique commonly employed by those who study orientation in stretched polymer networks[27] is to rotate the sample by 90°, thus producing a second set of equations with the polarization directions exchanged. Due to the technical difficulties created by the necessary optical acrobatics, we have instead chosen to assume that there is no preferential orientation within the plane of the surface. Therefore, $A_x = A_y$. The validity of this assumption may become questionable when flow-induced orientation could exist, such as during injection of the polymer solution into the cell. However, in the experiments presented here, we estimate that less than 1% of the total adsorbed mass diffused to the surface during the brief (4 s) injection process. The final objective, then, is to specify the mean segmental orientation, defined by the dichroic ratio $A_z/A_x = A_z/A_y$

$$D_{zx} = A_z/A_x = \alpha/\gamma(A_p/A_s - \beta/\alpha) \tag{3}$$

By this definition, a dichroic ratio of 1 indicates isotropy.

The carbon–hydrogen stretching region of the PMMA spectrum, shown in Figure 4, is dominated by the asymmetric methyl stretch at 3000 cm^{-1} and the symmetric methyl stretch at 2950 cm^{-1}. The solid line shows absorption from the p-polarized beam; the dashed line indicates adsorption from the s-polarization. The absorbance intensity of the s-polarized spectrum (quan-

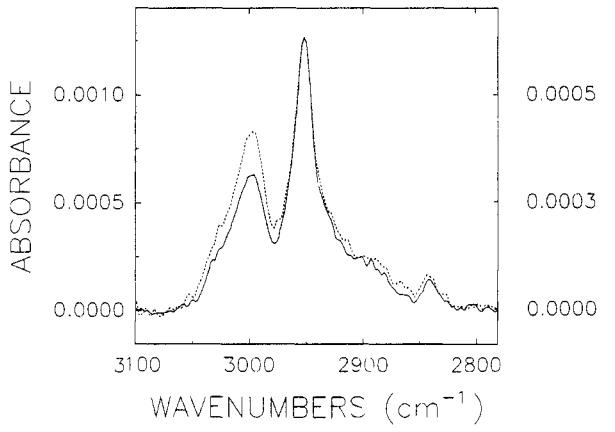

Figure 4. Infrared spectrum of h-PMMA adsorbed onto silicon oxide from a carbon tetrachloride solution of 0.01 mg/mL. The peaks centered at 3000 and 2950 cm^{-1} are primarily due to the asymmetric and symmetric CH_3 vibrations, respectively. The solid line (corresponding to the left vertical axis) shows the absorbance from the p-polarized beam, and the dashed line (right axis) indicates losses from the s-polarization. The absorbance intensity of the s-polarized beam has been scaled to correct for differences in electric field intensity. The peak at 2950 cm^{-1} (symmetric methyl stretch) is oriented randomly but the peak at 3000 cm^{-1} (asymmetric methyl stretch) has a dichroic ratio of 0.6.

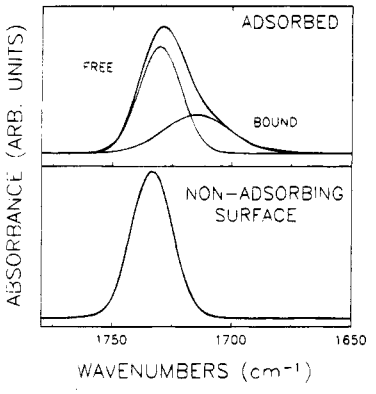

Figure 5. (Top) Asymmetrically shaped carbonyl peak of adsorbed h-PMMA (M_w = 90 000). It is composed of two constituent peaks. One peak is due to freely oscillating carbonyl groups located along the loops and tails which dangle into the solution. The other peak is due to carbonyl moieties that are hydrogen bonded to surface silanol groups and consequently have oscillations that are shifted to lower frequency. (Bottom) Corresponding spectrum of h-PMMA measured by ATR spectroscopy with a nonadsorbing surface, as described in the text. Note absence of the peak that reflects hydrogen bonding.

tified on the right axis) has been scaled by the ratio of electric field intensities in the p and s directions so that equal intensity on this plot implies isotropy. Therefore, we may conclude from this spectrum of adsorbed PMMA, under conditions described below, that the dipole transition moment of the symmetric peak is oriented randomly, while the asymmetric peak has a dichroic ratio of 0.6. Implications of this dichroism are discussed below.

Calibration of the Bound Fraction. The carbonyl peak of adsorbed PMMA (M_w = 107 000), shown as the asymmetrically-shaped line in Figure 5, is known to be composed of two constituent peaks.[28,29] One peak, centered at 1732 cm^{-1}, is due to freely oscillating carbonyl groups located along the loops and tails which dangle into the solution. The other peak, centered at 1710 cm^{-1}, is due to carbonyl moieties that are hydrogen bonded to silanol groups on the surface and consequently have oscillations that are shifted to a lower frequency. These peaks were resolved using SpectraCalc[30] software to generate a least-squares fit of a Gaussian to the free peak, and a Gaussian–Lorentzian mixture to the broadened bound peak. Throughout this study, we monitored the integrated intensities of the free and bound peaks in both polarizations. The bound fraction is given by $p = A_B(A_F + A_B)^{-1}$.

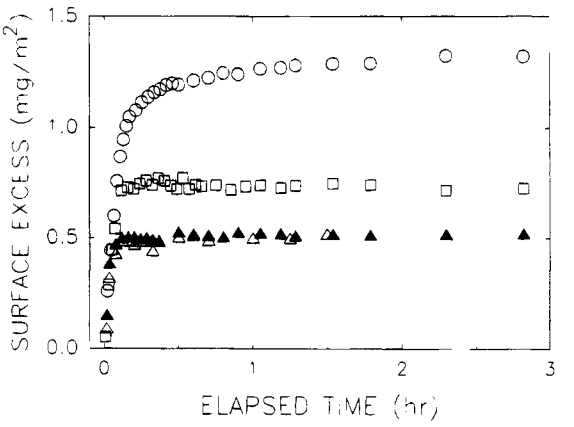

Figure 6. Illustration of the experiments described in sections I and II. Surface excess (mass $area^{-1}$) of h-PMMA (M_w = 90 000) is plotted versus time. First, the h-PMMA solution was exposed to the silicon surface. The ensuing growth of mass on the surface was followed for 3 h without interruption (circles). Other experiments began in a similar fashion, but included the exchange of the h-PMMA solution with d-PMMA (0.01 mg mL^{-1}, open symbols; 1.0 mg mL^{-1}, filled symbols) after 4 min (triangles) or 8 min (squares).

It has been shown that the molar absorptivity increases when the carbonyl becomes hydrogen bonded to the surface. Initially, we followed ref 29 in assuming that the molar absorptivity of the carbonyl is enhanced by 50% upon hydrogen bonding to the surface; later control experiments from this laboratory confirmed this presumption by direct measurement.[31] The bound fraction, for the data in Figure 6, is 0.3.

One could argue that the distinction between the free and bound peaks may be blurred by the effects of anomalous dispersion. This curse, which limits the accuracy of many ATR results when the intensity of absorbed radiation is large, could also in principle produce distortion of the absorption peaks. To quell these worries, we collected a spectrum of PMMA in solution by preventing adsorption of polymer with a methyl-terminated monolayer of condensed octadecyltriethoxysilane (OTE). The experimental method is described elsewhere.[26] The resulting spectrum of freely oscillating carbonyl groups, shown in Figure 5 (bottom), is clearly symmetric. Evidently, our absorption intensities were small enough to avoid the complication of anomalous dispersion.

Note that the true number of segments in intimate contact with the surface may be somewhat higher than reported here, as evidenced by ESR measurements in which the bound fraction is commonly reported to range from p = 0.5 to 0.8.[1] It has been suggested that the large disparity between IR and ESR measurements is due to segments bound to non-hydroxylic sites[1] to which infrared measurements are insensitive.

I. Immobilization of the Adsorbed Layer

A. Results. 1. Uninterrupted Adsorption of h-PMMA (M_w = 107 000). A simple experiment was devised to investigate the time evolution of segmental

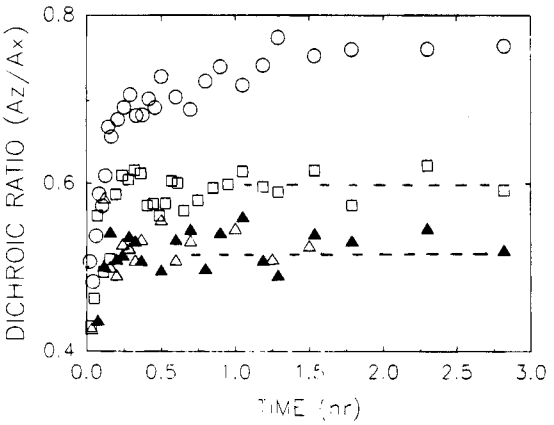

Figure 7. Dichroic ratios of the asymmetric CH_3 vibration versus elapsed time during the experiments shown in Figure 6. Triangles and squares represent experiments which included d-PMMA solution exchange after 4 and 8 min, respectively. Filled triangles again represent exchange with a solution concentration of 1.0 mg mL^{-1}.

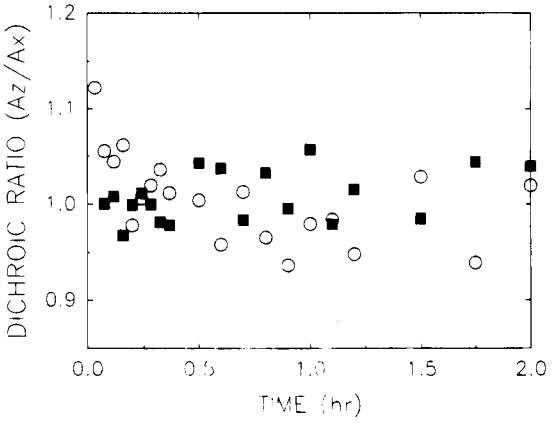

Figure 8. (Circles) Dichroic ratio of the symmetric CH_3 stretching vibration during the experiment described in section I. (Squares) Dichroism of the CD_3 stretches, averaged over four experiments to reduce scatter.

orientation, averaged over all chains composing the layer of h-PMMA (M_w = 107 000), during adsorption from dilute (0.01 mg mL^{-1}) CCl_4 solution. The circles of Figure 6 follow the growth of surface excess with time after the polymer solution was exposed to the substrate. Here the integrated intensities of the methyl stretches (see Figure 4), summed from both polarizations, were calibrated to give the mass adsorbed in mg m^{-2}. One sees that the adsorbed mass grew abruptly in early times, began to saturate after 20 min, and continued to slowly increase for the ensuing 3 h. Although other experiments with higher solution concentration varied in the rate at which a steady state level of adsorbed mass was reached, the steady state quantity of mass adsorbed did not change with changes in concentration. Therefore, these experiments were performed in the plateau region of the adsorption isotherm. The remaining symbols of Figure 6 are discussed in section II.

2. Selected Dichroic Ratios during Continuous Adsorption. We now embark on a brief tour of the mean segmental orientation of this layer. The time dependence of a collection of dichroic ratios, from various prominent infrared peaks in the spectra, are shown as the circles of Figures 7–9. Each will be addressed in sequence.

To begin, the circles of Figure 7 show the dichroic ratio of the asymmetric methyl stretch during adsorption. Two conclusions are drawn from this figure. First,

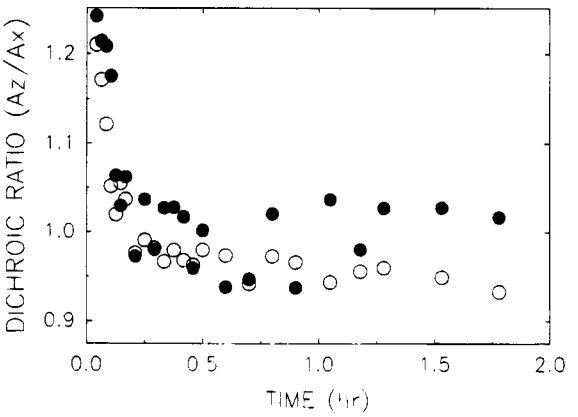

Figure 9. Dichroic ratios of the carbonyl vibrations during the experiment described in section I: open circles, free carbonyl; filled circles, bound carbonyl. This time-independent response was consistent for all of the experiments described in section II. The dichroic ratio is unity within the large experimental uncertainty.

the dipole transition moments of this vibration began with a large directional preference (D_{zx} = 0.5) in the plane of the surface and tended toward isotropy as time increases. Second, the time scale to reach steady state in dichroic ratio was similar to the time for achievement of equilibrium in mass adsorbed; both occurred with a characteristic time of ≈10 min.

Located at 2950 cm^{-1}, the symmetric methyl stretch responded less sensitively to changes in average orientation during adsorption. The circles of Figure 8 show that the dichroic ratio began at roughly 1.1 and quickly attained a steady state value of 1.0. By considering the normal modes of oscillation of this pyramidal CH_3 structure, it was expected that the orientation of the symmetric dipole transition moment would be approximately orthogonal to the orientation of the asymmetric transition moment. This expectation was borne out by the observation of inverse behavior of the dichroic ratios of these peaks. The relative magnitudes of segmental orientation observed in these peaks is discussed below.

The average dichroic ratio of the free carbonyl peak (open circles in Figure 9) fell from D_{zx} = 1.2 to 0.8 during the course of adsorption. Again, there appeared to be a strong correlation between the time to achieve a steady state dichroic ratio and the time to reach steady state of the total adsorbed mass. Though somewhat more scattered, the response from the bound peak (filled circles, Figure 9) showed signs of a similar decay from an orientation normal to the surface toward isotropy.

Finally, a word about the orientation of the bound carbonyl peak. We originally expected that the bound carbonyl stretching vibration would be oriented normal to the surface. After all, when averaged, the surface and the polymer layer are separated by only the z direction. Over the course of several experiments we found a slight preferential orientation normal to the surface (D_{zx} = 1.3), but it quickly became isotropic (Figure 9). We conclude that the constraints imposed by chain connectivity and surface roughness effectively scramble the orientations, thereby leaving isotropy, or near-isotropy, in its wake. The experimental scatter precludes definitive distinction between isotropy and near-isotropy.

3. Bound Fraction during Continuous Adsorption. Since each of these vibrations was separated from the chain backbone by at least one rotationally active

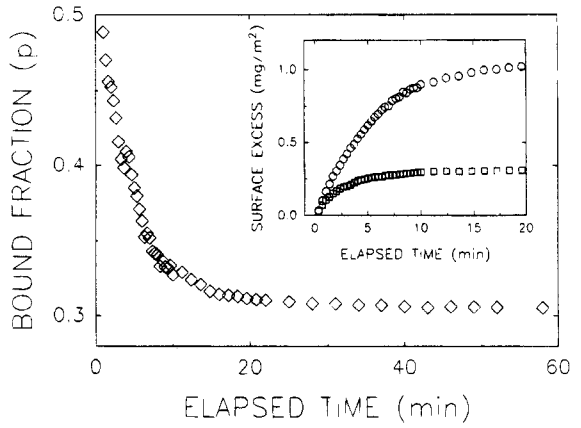

Figure 10. Time evolution of the bound fraction of h-PMMA (M_w = 90 000) during adsorption onto silicon from a carbon tetrachloride solution of 0.01 mg mL^{-1}. Inset: Surface excess of free (circles) and bound (squares) segments as indicated by curve-fitted intensities of the carbonyl peak (see text). These values were used to determine the bound fraction. The steady state bound surface excess corresponds to a coverage of hydroxyl groups amounting to roughly 6 per nm^2.

carbon–carbon bond, it was not possible to infer large scale molecular orientation given only the mean segmental orientation. To investigate the relation between the dichroic information and conformational properties of the entire chain, we used the methods described above to determine the fraction of segments per chain in hydrogen-bonded contact with the surface. Since motions on the monomeric length scale are required to precipitate changes in the bound fraction, this parameter provides a link between the monomeric and polymeric length scales. Although the bound fraction was monitored for each of the experiments described above, we show results only from an experiment which differed in the mode of data collection in order to obtain better time resolution. By collecting spectra in only one polarization, and employing the Bio-Rad kinetics software package,[32] we obtained enhanced time resolution without sacrificing signal quality. The inset of Figure 10 shows the time evolution of the free (circles) and bound (squares) carbonyl peak intensities. These data gave the bound fraction, $p = A_B(A_F + A_B)^{-1}$, discussed earlier in this paper. The bound fraction is shown as the diamonds of Figure 10. By inspection, one sees that the earliest chains attached nearly half of their segments soon after arrival at the surface. As more molecules reached the interface, the bound fraction, averaged over all chains composing the layer, fell off at a rate comparable to the rate of adsorption (Figure 6). The steady state average bound fraction was slightly greater than 0.3.

4. Analysis of the Uninterrupted Adsorption Experiment. With only the information given above, it was not possible to determine a unique mechanism for the observed time dependence of the bound fraction and mean segmental orientation. Two possibilities existed, depending on the surface mobility of the adsorbed chains. Suppose that mobility were enhanced so that relaxations from flat, tightly bound conformations were rapid on the time scale of diffusion of chains to the interface. While competing for surface adsorption sites, incoming chains would liberate previously adsorbed segments of recumbent resident molecules and allow expeditious evolution toward a more equilibrated and entropic structure. By the time steady state in total mass were reached, we might expect to have a homogeneous layer, though slightly flattened, with loops, trains, and tail structures conforming to the prescriptions of equilibrium thermodynamics.[1-3]

If, on the other hand, chain mobility were sluggish on the time scale of mass transport to the surface, then we might expect the flattened conformations to persist under a ponderous cover of more isotropic chains. In this scheme, only a fraction of potential adsorption sites would be left unoccupied by the flattened pioneering molecules. The later-arriving chains would adsorb to these few sites. A large dichroism and bound fraction would prevail initially, decaying as new chains contribute randomness to the averages.

The discrimination between these two possibilities is addressed in section II.

5. Isolation of the Early Chains. In this section we present results from a modified experiment, designed to distinguish between the alternative conformational structures described above. For the experiment represented by open squares of Figure 6, we allowed the h-PMMA to accumulate on the surface for only 8 min (4 min in the case of the open triangles). We then replaced the solution with d-PMMA (M_w = 90 000, c = 0.01 mg mL^{-1}) and allowed adsorption to proceed until the plateau mass was achieved (Γ = 3.2 mg m^{-2}). This gave us the ability to distinguish between the initial chains and those that arrived after 8 (or 4) min, thereby isolating a specific population of adsorbed molecules for measurement of dichroism.

6. Dichroic Ratio of Isolated Groups. The open triangles and squares of Figure 7 show the dichroic ratios for these two experiments. We find that the anisotropy was similar in each experiment at early times (starting at roughly 0.5), continuing as in the experiment described in section I. However, no further decay of the dichroic ratio, toward isotropy, was observed after the moment of solution replacement. The extent of anisotropic orientation of the pioneering chains remained frozen at that value and showed no signs of decay during our experimental time scale of 3 h.

By contrast, anisotropy of the deuterated methyl stretches was expected to decay as in the experiment of section I as d-PMMA saturated the surface. The dichroism of these peaks (located between 2300 and 1800 cm^{-1}) is shown as the squares of Figure 8. To reduce scatter, each data point has been averaged over four similar experiments. A literal inspection of the graph suggests that the deuterated layer arrived and remained isotropic, but this conclusion is not convincing because it was not possible to reliably resolve the symmetric methyl, asymmetric methyl, and methylene peaks. The small peak sizes gave unacceptably noisy results. No clear conclusion as to dichroism could be drawn.

As a control experiment, to evaluate the influence of d-PMMA on the orientation of the h-PMMA sublayer, a d-PMMA solution of much higher concentration (1.0 mg mL^{-1}) was used to displace the h-PMMA solution after 4 min (solid triangles, Figure 7). The orientation of the layer was apparently insensitive even to this drastic change in the environmental conditions.

7. Bound Fraction of Isolated Groups. The carbonyl stretches of deuterated chains could not be distinguished from those of protonated chains. We therefore expected, and observed, no changes in the behavior of the bound fraction or dichroic ratio of these peaks when d-PMMA solution was substituted for h-PMMA.

B. Discussion. The data from early adsorption times offers a clear picture of the initial condition of the pioneering chains. They diffused to the surface with a solution-like conformation and, upon arrival, were quickly adsorbed (more rapidly than our experimental resolution). Driven to maximize the number of segment−surface contacts, while paying an entropic cost, the initial molecules collapsed to a conformation with nearly half of their segments bound (see Figure 10). The effect of this flattened configuration was apparently manifested in the orientation of side groups. Infrared-active modes which show sensitivity to the chain orientation, such as the asymmetric methyl stretch and the free carbonyl stretch, provided evidence of a significant amount of orientation in the initial chains.

Figure 7 shows that this initial dichroism persisted for at least 3 h. The surprising inference is that there was no observable reorientation of the molecules composing this adsorbed layer. It is evident that the initial chains were forced to remain in a severely distorted conformation as later chains continued to anchor themselves to a diminishing number of surface sites. This overlayer, which adsorbed somewhat more isotropically, effectively obscured the flattened chains from our view in section I. The observation that different fractions of the layer resisted relaxation suggests that the entire structure was immobilized.

Previous work has shown spectacularly sluggish relaxations from nonequilibrium conformations. In a system characterized by weak interaction with the surface (polystyrene/cyclohexane/silicon oxide, $\chi_s = 2.1$) we found that a single time constant, τ_{off}, described displacement for a significant time (1−3 h), followed by a period of slower desorption kinetics. This behavior suggested the existence of distinct tightly and loosely bound populations.[12,13] An aging effect, in which τ_{off} continued to increase even after the mass adsorbed had equilibrated, implied surprisingly slow (hours to weeks) rearrangements of the loosely bound chains in the direction of conformational equilibrium. Far slower aging effects were found in experiments of sequential adsorption of h-PMMA/d-PMMA.[33]

Additional work in our laboratory[7−9] has shown that non-equilibrium states can be extremely long-lived when polymers of two different chemical compositions adsorb competitively. In a model system (PMMA adsorbed from CCl_4 onto oxidized silicon previously saturated with polystyrene, PS), it was shown that the weakly adsorbing PS was sterically pinned to a surface by the more strongly attaching PMMA. The dynamical evolution of the surface composition was strongly nonexponential in time and non-Arrhenius in temperature; the phenomenology was analogous to bulk glasses. In this system, the driving force for removal of the PS contained a contribution from the large difference in enthalpy of adsorption between PS and PMMA, a difference which did not exist in the present case of pure PMMA. We therefore expect that changes in composition and structure that occurred with a characteristic time of many hours in the PS−PMMA system should be dramatically slower in experiments with purely PMMA.

1. Immobilization due to High Density. Other demonstrations of immobilization of adsorbed macromolecules have appeared in the literature and deserve discussion. By studying the rheological behavior of a thin layer of polymer adsorbed to an air−water interface, Cohen Stuart and co-workers[34] found that it responded with a non-zero yield stress. The adsorbed layer was not fluid, but behaved as a surface gel. The most plausible interpretation is that creeping motions were precluded by the high density of segments within the first few monomers of the surface. It was suggested[5] that this effect, which was observed in a layer adsorbed to the *free surface*, should be common at a solid liquid interface. Indeed, computer simulations by Chakraborty and co-workers[35,36] of the diffusion of single chains on a surface, show dynamical behavior suggesting glasslike motion.

2. Immobilization due to Surface Interactions. These demonstrations of glassy surface properties illustrate the effect of steric constraints and segment−surface interactions on the center of mass diffusion of adsorbed chains. However, direct comparison with our observation of orientational stability is complicated by the difference in length scales probed. Evidence for immobilized train segments has been obtained using conventional high-resolution NMR.[37] In these experiments, the disappearance of the NMR signal due to mobile segments, as the surface coverage of PMMA was decreased, indicated highly restricted motion at the segmental level. ESR measurements of rotational correlation times of PMMA adsorbed to silica show that motions of segments in contact with the surface were 3 orders of magnitude slower than those located in the loops of adsorbed chains.[1,38] Rigid attachment at the segmental level was postulated.

3. Relationship between the Asymmetric and Symmetric CH_3 Stretches. When molecular models of the PMMA monomer are considered, it is puzzling that the asymmetric CH_3 stretch exhibited a large directional preference in the plane of the surface, while the symmetric CH_3 vibration appeared isotropic (see Figures 7 and 8). Indeed, one might naively expect that the extent of dichroism in these oscillations would be of equal intensity and in orthogonal directions. However, the complexity of the molecular architecture affords possibilities which could create this apparent paradox. The presence of separate methyl groups, located along the backbone and at the ester group, allows for a preferred relative orientation which, when the response of both groups are summed, could destroy the dichroism of one peak, while enhancing that of the other.

Another possibility is that the transition moment of the symmetric stretch could become preferentially aligned in a direction 45° to the surface. Thus, $A_x = A_z$. Nevertheless, the transition moment of the asymmetric stretch could prefer to lie in the plane of the surface. This complexity precludes quantitative determination of the extent of orientation. Experiments with PMMA that has been selectively deuterated to allow discrimination between the methyl and ester stretches would be useful in future work.

A more extended discussion[39] suggests that the observed dichroism likely reflects rotationally restrained ester groups of PMMA, specifically, segments that are directly in contact with the substrate (train segments).

II. Distribution of Conformations

Given the analytical methods presented in section I, the extent of orientation can only be determined as an average over the entire population of h-PMMA and d-PMMA. However, the specific distribution of chain orientations is also potentially a very valuable thing to know, though it has not (to our knowledge) been measured before. For example, a layer with a homo-

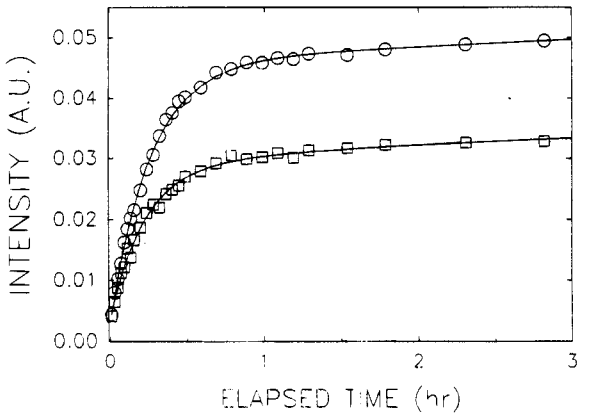

Figure 11. Integrated intensities of the absorbance from the p-(circles) and polarized s-(squares) infrared beams during adsorption of h-PMMA (M_w = 1.3 × 10^6) from carbon tetrachloride. The lines drawn through the data were obtained by a least squares fit of a double exponential function.

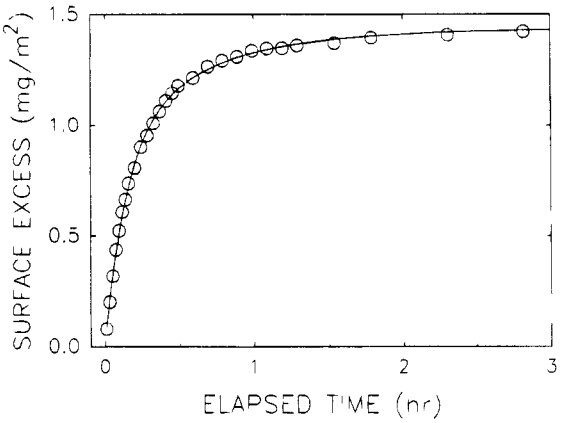

Figure 12. Illustration of the experiment described in section III. Surface excess of h-PMMA (M_w = 1.3 × 10^6) is plotted versus time after introduction to the bare silicon oxide surface. Slower kinetics allowed collection and coaddition of a greater number of scans per spectrum.

geneous distribution of conformations will have thermodynamic properties different from a similar layer containing distinct populations of tightly and loosely bound molecules. In this section we use the dichroic ratio of sequential groups of adsorbed molecules to construct an approximate distribution of conformations within the layer.

A. Orientation of Sequential Molecular Ensembles. The temporal stability of conformations made it possible to explore this distribution by calculating the dichroism of sequential groups of molecules as they arrived at the surface. The method was simple. We used a modification of eq 3 to calculate the dichroic ratio, where, instead of the overall absorbance, we now used only the absorbance contributed by an incremental mass adsorbed that arrived between t_i and t_{i+1}, so that

$$D_{zx} = \frac{\alpha}{\gamma}\left[\frac{A_p(t_{i+1}) - A_p(t_i)}{A_s(t_{i+1}) - A_s(t_i)} = \frac{\beta}{\alpha}\right] \quad (4)$$

As an approximation, the time assigned to each point corresponded to the average $(t_{i+1} - t_i)/2$. In a more careful treatment this average quantity would be weighted by the growth rate of surface excess, which is larger at the beginning of the time interval, but this possible correction is not believed to be significant.

Absorption increments $(A(t_{i+1}) - A(t_i))$ may be found in two different ways: by subtracting the spectrum collected at t_i from that collected at t_{i+1} and integrating to find the intensity of the difference spectrum, or by graphically fitting a smooth curve through the data in a plot of A_p and A_s versus time and subtracting the absorbance values from these curves. Both methods are described below. In the orientation data which follow, the circles represent graphical subtraction and the squares represent spectral subtraction.

This technique was first applied to the data of section I with inconclusive results. The rate at which surface excess grew with time forced a compromise in the number of scans per spectrum in order to maintain useful time resolution. The resulting data were too noisy to yield reliable conclusions. In this section, a similar experiment is described in which the kinetics of adsorption were slowed by using a polymer sample of higher molecular weight. Slower kinetics allowed us to co-add more scans per spectrum to reduce the amount of noise.

Shown in Figure 11 are the absorbances from the s-(squares) and p-polarized (circles) infrared beams, during adsorption of h-PMMA (M_w = 1.3 × 10^6) from dilute (c = 0.01 mg mL^{-1}) carbon tetrachloride. The segmental orientation, averaged over the entire adsorbed layer, was D_{zx} = 0.68 after 3 h. This increase in anisotropy, when compared with D_{zx} = 0.78 for the sample used in section I, reflects the tendency for chains of higher molecular weight to maintain a large bound fraction while accommodating many more segments in the interfacial region.[1] Calibration and summation of the absorbance intensities gave the surface excess, shown in Figure 12. The characteristic time to reach steady state in total mass adsorbed was nearly twice that for the sample used in section I.

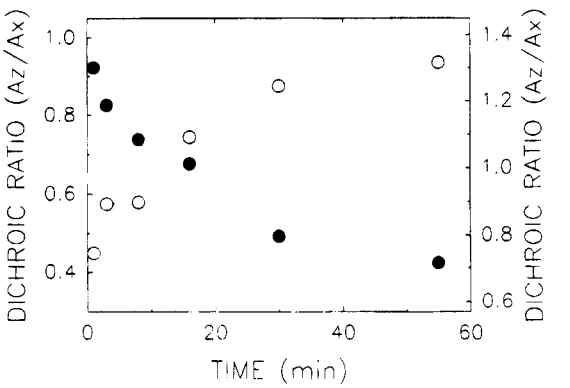

Figure 13. Histogram showing the dichroic ratios of sequential ensembles of adsorbed molecules versus the average time at which each group reached the surface. Open circles denote the asymmetric methyl stretch and refer to the left ordinate. Filled circles denote the free carbonyl peak and refer to the right ordinate. The data were obtained using the method of spectral subtraction described in the text.

Figure 13 is a histogram showing the dichroic ratios of sequential increments of mass, as determined by spectral subtraction (eq 4). Each data point corresponds to roughly 20% of the steady state adsorbed mass. The left axis follows the evolution of the asymmetric CH_3 stretch (open circles), and the right axis pertains to the free carbonyl vibration (filled circles). The dichroic ratios of the earliest group of molecules to arrive were $D_{zx}(CH_3)$ = 0.5 and $D_{zx}(CO)$ = 1.2. As expected, these values are equal to the initial dichroism of the experiment described in section I. Later doses of mass arrived with their average dichroic ratios adjusted in the same direction as observed in section I, but here the incre-

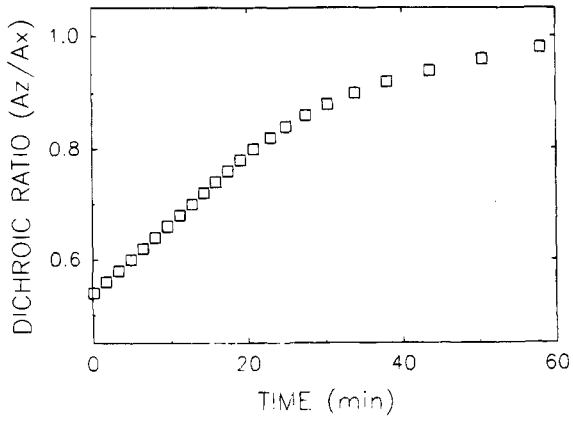

Figure 14. Dichroic ratio of sequential ensembles of adsorbed molecules versus the average time at which they reached the surface. This figure is identical to Figure 12 except that the incremental absorbances used in its derivation were obtained by graphical subtraction, resulting in a more precise curve-fit (see text).

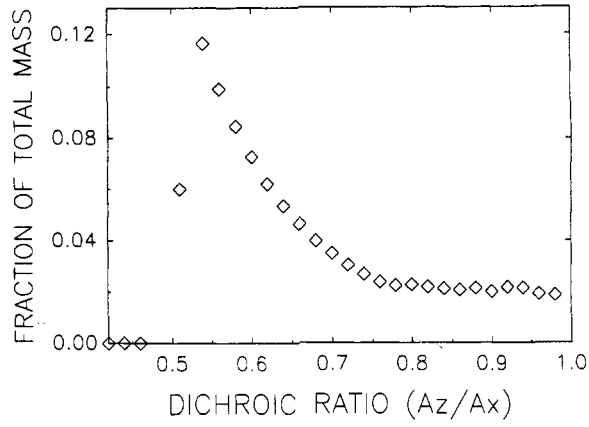

Figure 15. Histogram of the dichroism of the asymmetric CH_3 stretching vibration within the adsorbed layer. Determined from the data in Figure 14. The histogram was evaluated after the adsorption time of 40 min.

mental dichroism continued to evolve well beyond the previous saturation levels. The final group of molecules arrived with dichroic ratios of $D_{zx}(CH_3) = 1.0$ and $D_{zx}(CO) = 0.7$. When the incremental dichroism was averaged over all five data points, the steady state values observed in section I were recovered: $D_{zx}(CH_3) = 0.7$ and $D_{zx}(CO) = 1.0$.

B. Configurational Spectrum. 1. Histogram of Dichroism. The final objective was to construct a histogram showing the fraction of chains which occupy a given conformational state. In principle, this configurational spectrum could have been assembled using the data of Figure 13. Regrettably, these data were too sparse to produce a meaningful result. Instead, we constructed an idealization of the data in Figure 13 by performing the graphical absorbance subtraction, as described above. First, the absorbance data (Figure 11) were smoothed by adjusting the intensities to lie on the empirical line drawn through the data. The incremental absorbance to be used in the calculation of the dichroism (eq 4) was found by extracting consecutive differences from this idealized data. These sequential dichroic ratios were then plotted versus the average time of arrival for that increment of mass (Figure 14). Time increments for this plot were chosen to provide equal dichroic ratio increments of $\Delta D_{zx} = 0.02$, so that $D_{zx}(t_{i+1}) = 0.02 + D_{zx}(t_i)$. The data beyond 60 min were truncated due to the large propagation of error in this region. As the absorbance approached a steady state, the differences $(A(t_{i+1}) - A(t_i))$ approached zero, thereby creating wild fluctuations in the dichroic ratio. The quantitative similarity of the exact sequential dichroism (Figure 13) and the approximate sequential dichroism (Figure 14) confirms that this approximation scheme was valid for our purposes.

The information contained in Figures 12 and 14 was used to construct the configurational spectrum. First, Figure 14 gave the dichroic ratio of the ith ensemble of chains to arrive at the surface. The amount of mass contained in this ensemble was then found from the empirical curve fitted through the plot of mass versus time, by extracting consecutive differences from Figure 12, $\Delta\Gamma = \Gamma(t_{i+1}) - \Gamma(t_i)$. These increments were then normalized by the steady state value of adsorbed mass and plotted versus the dichroism of each increment in Figure 15. This histogram gave the fraction of mass in the mature layer which incorporates a given mean segmental orientation of the asymmetric CH_3 vibration. The upper limit of dichroism in this plot was limited by the propagation of errors as the incremental change in absorbance tended toward zero. The lower limit was restricted by the time resolution of our experiment.

2. Histogram of Bound Fraction. Just as for analysis of the dichroism, the key point allowing this further quantitative analysis was the assumption, validated by the experiments discussed above, that conformations were kinetically frozen. (This surely applied in a collective sense; adsorbed chains did not rearrange over experimental times, yet mobility of individual segments must be expected). In brief, the analysis was as follows. From the change of bound mass that resulted from a stipulated incremental mass of chains adsorbed, the quantity p' (the bound fraction of these chains) was determined by subtracting successive measurements. From these subtractions the histogram of the mass adsorbed, attributable to subpopulations of chains with different bound fractions p', was inferred. The lower limit of p' that could be inferred was restricted by the propagation of errors as incremental changes in the infrared spectra approached zero. The upper limit of p' was restricted by the time resolution, $\approx$1 min, of the experiment.

Figure 16 shows the resulting histogram for the experiment of Figure 14. As in Figure 14, the histogram is severely asymmetric; there are distinct populations of chains, those that adsorbed first and those, more tenuously adsorbed, that adsorbed later.

Parenthetically, we note that the distribution calculations are made on the hypothesis of total conformational stability. Figure 7 shows that this is correct at the earlier stage of adsorption, when polymers have the opportunity to arrange many surface–segment contacts, so the structure is frozen. It is true that chains deposited at a very high surface coverage have fewer surface contacts, and such loosely bound polymers might experience exchange between bound and loop portions, but this does not affect the conclusion (see section below on Future Prospects) as to bimodality.

3. Discussion. As expected, when these data were summed to find the area under the curves, we recovered the mean segmental orientation and bound fraction of the entire layer. The most striking feature of these histograms is their asymmetry. Upon inspection, one sees that a very large fraction of the chains, roughly 50%, was confined to conformations with dichroic ratio between $D_{zx} = 0.55$ and 0.65. Very few molecules, less

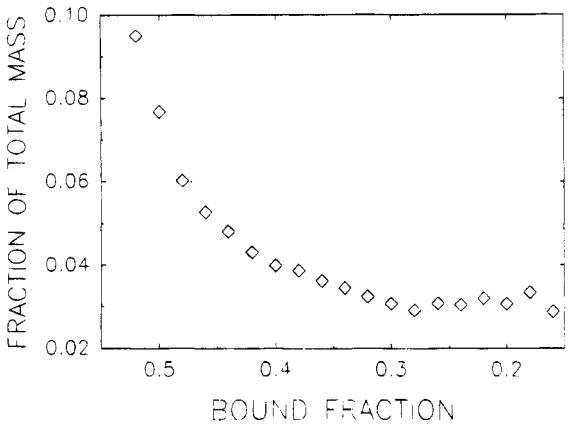

Figure 16. Histogram of the bound fraction evaluated after the adsorption time of 40 min. Determined, for bound fractions separated by $Dp' = 0.02$, from the data in Figure 10. This histogram actually splits to become bimodal if evaluated at later times. One population is composed of those chains, shown in this figure, that meet a bare surface and sink into highly-flattened configurations. The second population is composed of those chains that, meeting a nearly-saturated surface, became attached more tenuously.

than 5%, exhibit a greater amount of anisotropy, while the other half of the layer found its dichroism spread evenly from $D_{zz} = 0.65$ to 1.0. Similar conclusions hold for the bound fraction.

The evidence presented here gives quantitative support to speculative conclusions that have previously appeared in the literature. On the basis of influence of chain conformations on measurable of thermodynamic quantities, such as the surface excess and exchange kinetics, Varoqui, Pefferkorn, and co-workers concluded that the earliest arriving chains were tightly adsorbed into a quasi two-dimensional state and that later chains adsorbed more loosely.[10,11] This is reminiscent of qualitative ideas suggested by Furusawa and co-workers[40,41] and by Grant, Passaglia, and Smith.[42-44] Previous studies in our laboratory of polymer exchange kinetics in polystyrene systems also implied a distribution in the manner in which the polystyrene adsorbed; a bimodal distribution was proposed, with a time-dependent ratio of tightly and loosely bound molecules.[13,14] The present experiments have quantified this distribution in a favorable model system and show it to be continuous and unimodal.

These distributions of surface localization energy and molecular shape quantify the role of kinetic history in forming the final structure of the adsorbed layer and restricting its later mobility. The polymer chains diffused to the initially-bare surface in a random-coil configuration and, in initial spreading processes (more rapid than the time resolution of this experiment), sank into flattened conformations with almost 50% of the segments hydrogen bonded to the surface. It is remarkable that chains with random-coil radius of gyration ≈30 nm could, so quickly, do this. Chains that adsorbed later, finding fewer and fewer surface sites available, then became attached by fewer and fewer segments. This in turn implies that chains which arrived first had the center-of-mass closer to the solid surface than those which arrived later.

The significance is that traditional models of these phenomena present the adsorbed layer as having a unique equilibrated structure that may be predicted solely upon the basis of the relative free energies of interactions;[1-3] in spite of speculation about nonequilibrium structures for many years, the experimental situation was confused owing to insufficient experimental ability to discriminate between various proposed explanations.[1-4] But it is clear in principle that a path toward the lowest-energy state might not be available. This study has provided the first direct confirmation of the expectation and has shown a method to map out the distribution of conformational substates that characterizes nonequilibrated surface structures. Rather, the interpretation is suggested (see section which follows) that these nonequilibrated surface structures originate from a process of piecemeal surface deposition.

III. Future Prospects

After this study was completed, further studies extended this method of evaluating the histogram of adsorbed states and led to the important conclusion that when the histogram of PMMA adsorption was evaluated at times later than shown in Figures 15 and 16, those broad distributions actually split to become bimodal.[45,46] One population was composed of those chains that met a bare surface and sank into highly-flattened configurations (Figures 15 and 16). These chains had the opportunity to arrange many surface-segment contacts and their structure was effectively frozen in time. The second population was composed of those chains that, meeting a nearly-saturated surface, became attached more tenuously.

Further studies using a different approach led to similar conclusions for PS (polystyrene) adsorption from carbon tetrachloride.[46,47] In this system the adsorption is significantly weaker than for PMMA. On the experimental side, this then shows that the conclusion could find wide applicability.

Note that most other experimental techniques used to characterize the polymer surface structure determine an averaged structure and are blind to this actual distribution of adsorption substates.

This evokes problems of other scientific fields: the "parking problem" and random sequential adsorption. Here objects are deposited onto a plane one by one with random locations except that the same spot cannot be occupied by the same object.[48-50] This is normally considered for rigid objects. Flexible polymers can continue to adsorb by adjusting their shape to adsorb at fewer and fewer surface sites. Shape flexibility of polymer chains affords a mechanism for surface coverage to reach unity, unlike the oft-analyzed case of rigid objects.[48-50] This picture of piecemeal surface deposition contrasts strongly with the expected intertwining of polymers at conformational equilibrium. An interesting implication is that the chains which adsorbed later, finding fewer and fewer surface sites available, and becoming attached by fewer and fewer segments, should have had the center-of-mass located farther from the adsorption surface than those which arrived first. These chains might most influence the oft-studied[1-3] hydrodynamic thickness.

Acknowledgment. The authors are indebted to H. Schneider and E. Enriquez for collaborations and discussions about this work. Support was provided through the National Science Foundation (Polymers Program), Grant NSF-DMR-91-01509.

References and Notes

(1) Fleer, G. J.; Cohen Stuart, M. A.; Scheutjens, J. M. H. M.; Cosgrove, T.; Vincent, B. *Polymers at Interfaces*; Chapman and Hall,New York, 1993.

(2) Kawaguchi, M.; Takahashi, A. *Adv. Colloid Interface Sci.* **1992**, *37*, 219.
(3) de Gennes, P.-G. *Adv. Colloid Interface Sci.* **1987**, *27*, 189.
(4) Granick, S. In *Physics of Polymer Surfaces and Interfaces*; Sanchez, I., Ed. Manning Publications: New York, 1993.
(5) de Gennes, P.-G. In *New Trends in Physics and Physical Chemistry of Polymers*; Lee, L.-H., Ed. Plenum Press: New York, 1990.
(6) Johnson, H. E.; Granick, S. *Macromolecules* **1990**, *23*, 3367.
(7) Johnson, H. E.; Granick, S. *Science* **1992**, *255*, 966.
(8) Johnson, H. E.; Douglas, J.; Granick, S. *Phys. Rev. Lett.* **1993**, *24*, 3267.
(9) Douglas, J. F.; Johnson, H. E.; Granick, S. *Science* **1993**, 262, 2010.
(10) Pefferkorn, E.; Haouam, A.; Varoqui, R. *Macromolecules* **1988**, *21*, 2111.
(11) Pefferkorn, E.; Haouam, A.; Varoqui, R. *Macromolecules* **1989**, *22*, 2677.
(12) Frantz, P.; Granick, S. *Phys. Rev. Lett.* **1991**, *66*, 899.
(13) Frantz, P.; Granick, S. *Macromolecules* **1994**, *27*, 2553.
(14) Schneider, H. M.; Granick, S. *Macromolecules* **1992**, *25*, 5054.
(15) Schneider, H. M.; Granick, S.; Smith, S. *Macromolecules* **1994**, *27*, 4714.
(16) Schneider, H. M.; Granick, S.; Smith, S. *Macromolecules* **1994**, *27*, 4721.
(17) Flournoy, P. A.; Schaffers, W. J. *Spectrochim. Acta* **1966**, *22*, 5.
(18) Van Alsten, J. *Macromolecules* **1992**, *25*, 3007.
(19) Sung, C. *Polym. Prepr. (Am. Chem. Soc., Div. Polym. Chem.)* **1990**, *31*, 521.
(20) Frantz, P.; Granick, S. *Langmuir* **1992**, *8*, 1176.
(21) Dijt, J. C.; Cohen Stuart, M. A.; Fleer, G. J. *Macromolecules* **1992**, 25, 5416.
(22) Harrick, N. J. *J. Opt. Soc. Am.* **1965**, *55*, 851.
(23) Harrick, N. J. *Internal Reflection Spectroscopy*; Interscience; New York, 1967.
(24) Tompkins, H. G. *Appl. Spectrosc.* **1974**, *28*, 335.
(25) Azzopardi, M. J.; Arribart, H. *J. Adhesion*, in press.
(26) Kessel, C. R.; Granick, S. *Langmuir* **1991**, 7, 532.
(27) Kaito, A.; Nakayama, K. *Macromolecules* **1992**, *25*, 4882.
(28) Fontana, B. J.; Thomas, J. R. *J. Phys. Chem.* **1961**, *65*, 480.
(29) Lee, J. Y.; Painter, P. C.; Coleman, M. M. *Macromolecules* **1988**, *21*, 346.
(30) Galactic Industries, Salem, NH.
(31) Schneider, H. M.; Granick, S. Unpublished.
(32) Bio-Rad Laboratories, Digilab Division, Cambridge, MA.
(33) Johnson, H. E. Ph.D. Thesis, University of Illinois at Urbana–Champaign, 1992.
(34) Cohen Stuart, M. A.; Keurentjes, J. T. F.; Bonekamp, B. C.; Fraaye, J. G. E. M. *Colloids Surf.* **1986**, *17*, 91.
(35) Adriani, P. M.; Chakraborty, A. K. *Macromolecules* **1992**, *25*, 2470.
(36) Chakraborty, A. K.; Shaffer, J. S.; Adriani, P. M. *Macromolecules* **1991**, *24*, 5226.
(37) Sakai, H.; Fujimori, T.; Imamura, Y. *Bull. Chem. Soc. Jpn.* **1980**, *53*, 3457.
(38) Miyamoto, T.; Cantow, H. J. *Makromol. Chem.* **1972**, *162*, 43.
(39) Enriquez, E.; Schneider, H. M. Granick, S. *J. Polym. Sci., Polym. Phys. Ed.*, in press.
(40) Furusawa, K.; Yamashita, K.; Konno, K. *J. Colloid Interface Sci.* **1982**, *86*, 35.
(41) Furusawa, K.; Yamamoto, K. *J. Colloid Interface Sci.* **1983**, *96*, 268.
(42) Stromberg, R. R.; Grant, W. H.; Passaglia, E. *J. Res. Natl. Bur. Stds.* **1964**, *68A*, 391.
(43) Stromberg, R. R.; Tutas, D. J.; Passaglia, E. *J. Phys. Chem.* **1965**, *69*, 3955.
(44) Grant, W. H.; Smith, L. E.; Stromberg, R. R. *Faraday Discuss Chem. Soc.* **1975**, *59*, 209.
(45) Schneider, H. M.; Frantz, P.; Granick, S. Submitted for publication.
(46) Schneider, H. M. *Ph.D.* Thesis, University of Illinois at Urbana–Champaign, 1995.
(47) Schneider, H. M.; Granick, S. Submitted for publication.
(48) Evans, J. W. *Rev. Mod. Phys.* **1993**, *65*, 1281.
(49) van Tassel, P. R.; Viot, P.; Tarjus, G.; Talbot, J. *J. Chem. Phys.* **1994**, *101*, 7064.
(50) Ramsden, J. J. *Phys. Rev. Lett.* **1994**, *71*, 295.

MA9503064